Investigation on Compressibility and Microstructure Evolution of Intact Loess During Wetting Process

Tao Jian
Wuhan Institute of Rock and Soil Mechanics Chinese Academy of Sciences
Ling-wei Kong
Wuhan Institute of Rock and Soil Mechanics Chinese Academy of Sciences
Wei Bai (william_bai@yeah.net)
Wuhan Institute of Rock and Soil Mechanics Chinese Academy of Sciences
Zhi-liang Sun
Wuhan Institute of Rock and Soil Mechanics Chinese Academy of Sciences

Research Article

Keywords: intact loess, water content, compressibility, microstructure, SEM, MIP

Posted Date: December 28th, 2021

DOI: https://doi.org/10.21203/rs.3.rs-1026244/v1

Abstract

Loess is widely deposited in arid and semi-arid areas and is characterized by low dry density, developed pore space, and loose structure, which is not commensurate with that high structural strength and shear strength in the dry state. Many natural phenomena and experimental studies show that intact loess is very sensitive to the change of water content, with slight increases in water content causing a rapid reduction in strength. Abundant information is available in the literature for collapsibility of loess; however, the research on the evolution of loess compressibility during wetting is still minimal, which is very helpful to understand the loess collapsible deformation caused by long-term irrigation. In this paper, the evolution of compressibility of intact loess during wetting are studied by oedometer test, and the microstructure and pore size distribution (PSD) is characterized on intact loess specimens with different water content before and after oedometer tests by scanning electron microscopy (SEM) and mercury intrusion porosimetry (MIP) methods. The results show that the compression index (C_c) and secondary compression index (C_α) of intact loess depend on water content and vertical stress and change abruptly after the vertical stress exceeds the yield stress. The C_α/C_c values of the intact loess are not constant, which increased with the vertical stress to peak and then gradually decreased and tend to 0.025. Both wetting and loading can cause microstructural damage to the intact loess, in which loading leads to the collapse of the overhead structure and transformation from a bimodal PSD into a single PSD, and wetting intensifies the collapse of microstructure to form a compacted interlocking structure and promotes the transformation of medium pores into small pores.

Introduction

Loess is aeolian sediment in arid and semi-arid areas, which is widely distributed in Africa (Nouaouria et al.,2008), South America (Francisca,2007), North America (Saye et al.,1988), Europe (Bally,1988), Oceania (Yates et al.,2018) and Asia (Youssef et al.,2013; Sadeghi et al.,2019; Zhang et al.2019), especially in the Loess Plateau of China, with continuous distribution and enormous thickness (Liu,1985). The unique material composition, depositional environment, and depositional mode make the loess form the metastable structure of weak cementation and high porosity, among which the aggregate particles and overhead structure are the most typical characteristic. The metastable structure of loess has a defining role of collapsibility and compressibility when wetted and loaded (Gao,1988; Assallay et al.,1997; Li et al.,2016). Natural loess with low moisture content shows high strength and keeps stable; however, even if wetted slightly, its strength will decrease sharply, resulting in the destruction and collapse of the structure under loading, not to mention inundated (Wen et al., 2014; Yates et al.,2018). Numerous geological disasters in the loess area are closely related to the great deformation caused by loess wetted, such as differential settlement (Hou et al.,2019), earth cracks (Lu et al.,2019), and destruction of infrastructures (Saye et al.,1988; Bally,1988). With the development of society, human activity on the rise in the Loess Plateau will bring more potential problems of loess collapse caused by wetting. Among them, long-term irrigation activities are the most important factor for the frequent occurrence of geological disasters (such as landslide and land subsidence) in the loess tableland (Juang et al.,2019). However, compared with

landslides (Xu et al.,2014; Leng et al.,2018), the available literature on land subsidence caused by long-term irrigation is very limited (Hou et al.,2019).

Since the last century, geotechnical practitioners and researchers have focused on and studied the problem of loess collapsible deformation due to wetting. Many pieces of research have proposed the method of measuring the collapsibility coefficient by double oedometer and soaking triaxial test (Reznik, 1992; Jiang et al.,2012), summarized the relationship between soil physical and mechanical properties and collapsibility (Handy,1973; Grabowska-Olszewska,1989; Francisca,2007; Sadeghi et al.,2019; Zhang et al., 2019), suggested the prediction model of loess collapsibility (Xie et al.,2018; Hou et al.,2019; Wang et al.2020b), tried to clarify the collapsible mechanism based on the mineral composition and microstructure of loess (Barden et al.,1973; Assallay et al.,1997; Dijkstra et al.,1995; Smalley and Marković,2014; Liu et al.,2016; Li et al.,2016), and estimated the in-situ loess collapsibility deformation through the loess collapsibility coefficient measured in the laboratory(Shao et al.,2015). The main focus of the literature reported works had been laid on the characteristics and mechanism of the instantaneous collapse of loess during inundating. However, it is difficult to estimate accurately the loess settlement deformation caused by long-term irrigation with the results of the loess collapse test in the laboratory. The main reasons are as follows: (1) within the influence range of irrigation infiltration, the water content of soil increases, but the soil is nearly saturated only in the surface layer (Hou et al.,2018); (2) the variation in soil properties caused by the development of wetting deformation; (3) this is a long-term process, and the secondary compression of soil should not be ignored. Therefore, to accurately estimate the settlement deformation due to long-term irrigation, a clearer understanding of the evolution of the compressibility of intact loess during the wetting process is required. Limited information is found in the literature for wetting deformation of loess, which introduced the relationship between wetting deformation coefficient and influencing factors (such as vertical stress, properties of loess, and wetting water content),and only for remolded loess (Yang et al.,2017).

It is well known that the microstructure significantly influences the hydro-mechanical behavior of loess. However, the evolution of the microstructure of loess is still unclear during wetting and loading. The evolution information of loess microstructure under wetting and loading is helping to fully understand the compression deformation characteristics of loess and provide a forceful basis for the constitutive model that can better fit the hydro-mechanical behavior of loess (Wang et al., 2018, 2020a). Particle pattern, contact relation, bonding material, and pore size distribution are the key factors of metastable loess microstructure, and it is significant to accurately characterize them for understanding the deformation of loess due to wetting (Gao,1980a, 1980b; Li et al.,2016). Since scanning electron microscope (SEM) was used to observe the microstructure of soil, which has played an important role in observing the particle morphology, interparticle cementation, and size and shape of the pore. In addition, the SEM images are processed by image processing software to acquire the quantity information of microstructure (Li and Li,2017; Li et al.,2019), but this work is extremely cumbersome, and there are some subjective on the distinction between particles and pores (Li et al.,2016; Wang et al.2018,2020a). Mercury intrusion porosimetry (MIP) is a reliable technique for measuring pores of the soil. Although the original structure of loess may be destroyed during the early intrusion, many studies have successfully measured the pore

size distribution of loess using the MIP method (Lei et al.,1987; Jiang et al.,2014; Ng et al.,2016; Shao et al.,2018; Wang et al.,2018, 2020a). The combination of the two micro testing techniques can fully and accurately characterize the microstructure of loess, which has been applied in the understanding of loess microstructure (Lei et al.,1987), the analysis of microstructure evolution of loess during shearing and collapsing (Jiang et al.,2014; Shao et al.,2018; Li et al.,2020), and the microstructure evolution of undisturbed, remolded and saturated loess under loading (Ng et al.,2016; Wang et al.,2018, 2020a). The water content of intact loess greatly influences its compressibility, but there are still some insufficient in understanding, that is, the influence of water content on the microstructure of intact loess and microstructure evolution during wetting and loading.

This paper presents the results of oedometer tests performed on intact loess with different water content, focusing on the evolution of the compressibility of intact loess under wetting and loading. And to further explore the mechanism of compression response, the microstructures of intact loess specimens with different water content before and after compression are characterized by SEM and MIP techniques, which are compared and analyzed for the evolution of the particle contact relation and pore size distribution.

Study Area And Samples

Lanzhou is located in the northwest of the Loess Plateau in China, where the thick loess distributes entirely in terms of geology, where the three main stratigraphic units of loess are named the Wucheng loess(Q_1), the Lishi loess(Q_2), and the Malan loess(Q_3) separately. All loess samples were excavated by utilizing hand tools at a depth of 3-4m below the top of the slope, which is Malan loess and has a yellow color (Fig.1(a)). The excavated loess blocks are carefully cut into cubes with 25cm and immediately packeted in clingfilm. It was then wrapped in a plastic membrane and coated with melted paraffin. Finally, placing the wrapped block in a specifically designed wooden box equipped with shock absorption foam on all inner sides (Fig.1(b)). This work is done so that the samples maintain natural moisture content as much as possible and do not break during transport.

Some basic physical properties of the loess samples are summarized in Table 1. The intact loess is relatively dry with a moisture content of 7.14%, a low dry density of 1.396g/cm^3. The specific gravity, liquid limit, and plastic limit of studied loess were tested as 2.78, 29.7%, 17.9%, respectively. According to the classification of loess proposed by Gibbs and Holland (Gibbs and Holland,1960; Liu et al.,2016), the studied loess belongs to silty loess (Fig.2). The particle size distribution (Fig.3) was tested by particle size analyzer Mastersizer 2000, which showed that the loess is dominantly composed of silt, accounting for 80.78%. Also, it contained a small amount of clay (10.36%) which had a significantly dominating effect on the mechanical behavior of loess (Cilek,2001; Smalley and Marković,2014; Li et al.,2016). The mineralogical composition of the loess was obtained by X-ray diffraction (XRD), which consist mainly of a large number of non-clay minerals (quartz, albite, calcite), accounting for more than 78%, in which the calcite (13.23%) needs to be focused on, some studies have shown that calcite is an essential part of enhancing the mechanical strength of the loess (Wen and Yan.,2014; Meng and Li, 2019; Pihlap et

al.,2021). It also contains some clay minerals, which are also critical cementing materials, mainly illite at 14%, and the cementation of clay minerals and secondary calcite is an essential factor in the formation of the metastable structure of loess (Cilek,2001; Smalley and Marković,2014; Li et al.,2016; Liu et al.,2016).

Sample preparation and methods

Sample preparation

Compression specimens were extracted from the block sample with steel rings of 61.8mm in diameter and 20mm in high, which had a natural water content of 7.14%, the other specimens are wetted by adding distilled water onto the natural specimens to a saturation degree of 30%, 40%, 50%, 60%, 70%, 80%, 90%, respectively, and saturated specimen obtained by vacuum saturation approach. The wetted specimens were wrapped in cling film and placed in a moisture chamber for one week to allow sufficient water uniformity. The initial state of each specimen is shown in Table 2.

Compression test

Xie (2016) concluded that the total amount of deformation of loess when it is wetted to certain water moisture under a certain pressure is independent of the stress path, the wetting path, and the sequence of loading and wetting. Therefore, for specific loess, the pore ratio after wetting and compression are unique, and Shao et al. (2018) used this method to study the wetting collapse characteristics of remolded loess. In view of this, this paper carries a wetting compression test by wetting and then loading the intact loess specimens. The specimens were installed in the consolidation box, and a moist cotton cloth was stuffed into the water tank of the box to reduce the evaporation of the unsaturated sample, and the saturated specimen were filled with water in the water tank. Then the axial displacement transducer and check that all parts are in contact. Finally, turning on the data acquisition system and loading. The loading paths for each specimen are 12.5kPa, 25kPa, 50kPa, 100kPa, 200kPa, 400kPa, 800kPa, 1600kPa, 3200kPa. The compression test stability standard was 24 hours after loading (Chinese National Standards GB/T 50123-2019). For secondary compression stability standard, the loading time extended under each loading until the axial deformation was less than 0.002mm per day (Ge et al.,2015). After the test, the specimen was carefully taken out from the apparatus, freeze-dried for microstructure tests. The state of each specimen after compression is shown in Table 2.

Microstructure test

The microstructure of intact loess due to wetting and the microstructure evolution state of loess with different saturation after compressing were observed and compared using SEM and MIP, focusing on particle morphology, contact relation, cement materials, and pore size distribution. Five specimens were observed, including natural and saturated loess and compressed intact loess, 50% saturated and saturated loess, which were dried by the freezing method to reduce the damage to microstructure during the specimen preparation.

Cubic bars with the dimensions of 2cm×1cm×1cm(length×width×height) were carefully cut off from the dried specimens, and which were broken from the middle to reveal a fresh surface and coated with gold for SEM tests. A series of SEM images with different magnifications were taken of each sample to observe the morphology of the particle distribution and the details of the particle contact.

The samples of MIP were cubes with the dimensions of 1cm, which were trimmed out from dried specimens as same as that for SEM samples. Mercury is a non-wetting fluid that requires external pressure to intrude into the pore of soil, which will progressively intrude into tinier pores as the pressure increases, and the intrusion volume of mercury and intrusion pressure can be continuously monitored. A simplified assumption that pores are cylindrical, the relationship between the intrusion pressure and the intruded pore diameter can be written as: $P=-4\gamma\cos\theta/D$, where P is the pressure that the mercury can intrude into the pore with the diameter of D, γ is the surface tension of mercury, and θ represents the contact angle of the mercury with the pore walls. In this study, γ=0.485N/m, θ=130°, mercury intrusion pressure in MIP instrument from 0.52psia to 54955.09psia.

Results And Discussion

Evaluation of compressibility

Benatti and Miguel (2013) proposed the structural models for colluvial and lateritic soil based on their three stages of collapsible behavior, taking into account the effects of matrix suction and cementation. Analogously, intact loess also has typical characteristics of unsaturated and intergranular cementation. As shown in Fig.4, the compression of loess can be divided into three stages in e-logσ_v coordinates: (Ⅰ) The skeleton particles become tighter, with mild linearly decrease in void ratio at small vertical stress; (Ⅱ) Gradually breakage of interparticle cementations and aggregates, the collapse of the overhead structure, with decreasing void ratio at an increasing rate of change in void ratio at intermediate vertical stress; (Ⅲ) Completely breakage of interparticle cementations and aggregates, particles rearrangement, with decrease sharply in void ratio at great vertical stress. However, it is worth noting that these stages are not completely separated, for example, there are also cementation breakage and particle moving in stage Ⅰ, only that elastic compaction is predominant. A curved connection (Stage Ⅱ) between two straight lines (Stage Ⅰ and Stage Ⅲ) indicates that the interparticle cementation gradually fractures with increasing vertical pressure. In ln(1+e)-logσ_v plane, the pore ratio varies nearly linearly with increasing vertical pressure in the two phases of elastic compaction and particle rearrangement, and the vertical pressure corresponding to the intersection of the two linear segments is determined as yield stress (Sridharan et al.,1991; Cheng et al.,2020; Leng et al.2021).

Fig.5(a) shows the compression curves of intact loess with different initial water contents in the e-logσ_v plane. The void ratio of all specimens decreases with vertical stress; with the same initial pore ratio, the higher the initial water content, the faster the void ratio decreases. Following the method proposed by Sridharan et al. (1991), the yield stress of intact loess with different initial water content determined and showed in Fig.5(b), (c), (d), when the water content of specimens is low, the two straight sections are

evident (Fig.5(b)); when the water content of specimens are very high, the slop of the two straights is almost the same (Fig.5(d)). The intersection of two lines gradually moves to the left as the water content increases, meaning that the higher the water content, the smaller the yield stress of the intact loess. The yield stress decreases sharply and then stabilizes as water content increases, as shown in Fig.6, which relationship can be well fitted by the power function based on water content w_0. This result is consistent with the conclusion of other papers (Chen et al.2006; Leng et al.2021), presented in Fig.6. It is also worth noting that the yield stress of the intact loess is approximately 530kPa, which is significantly higher than the cover earth pressure, and they (Munoz-Castelblanco et al.,2012; Sadeghi et al.,2019) presumed that the apparent over-consolidation should be related to the soil-forming process, where the cementation between the skeletal particles provides great cohesion.

The compression index (C_c) is the slope of the compression curve that can be defined as $C_c = \Delta e / \Delta \log \sigma_v$, which evolves with vertical stress to evaluate the compressibility of the intact loess. Fig.7 shows the variation curve of the compression index with vertical pressure, and it can be seen that the compression index of each specimen increases with increasing vertical pressure. However, the evolution of the compression index of specimens with different water contents follows different paths. The compression index of loess with low water content loess increases slowly and then sharply with vertical stress, whereas the compression index of loess with high water content is high and increases rapidly before becoming slow. Further observation of the evolution of compression index shows that the difference of evolution path of compression index seems to be related to yield stress, when the vertical stress exceeds the yield stress, the compression index will increase greatly. The evolution of the compression index with vertical stress is related to the yield stress, which is similar in other soils (Perisic et al.,2019; Rezania et al.,2020). The further increase of compressibility of low water content loess after the vertical stress exceeds the yield stress may arise from two aspects: one the one hand, from the fracture of the inter-particle cementation, the sudden reduction in strength and a great deal of compression space remains after the previous loading; on the other hand, the increase in saturation due to volume compression also contributes to the compressibility of unsaturated soil(Rezania et al.,2020), as can be seen from Table 2, although the water content of the specimen decreases after compression, the saturation increases.

Evaluation of secondary compressibility

The compression of soils consists of two stages: the primary compression stage, in which the effective stress is increased by the extrusion of pore water and pore gas resulting in the soil volume being compressed; and the secondary compression stage, in which the effective stress is constant and packing density of soil particles increases slowly with time (Mitchell et al.,2005). The study of the secondary compression characteristics of soils is of great significance in evaluating the long-term stability, especially in the loess areas of China, when evaluating the settlement deformation caused by long-term irrigation in loess tableland, the secondary compression deformation can not be ignored.

It is not easy to determine accurately and quickly the demarcation point of primary and secondary compression in the void ratio versus the logarithm of time(e-logt). Mataic et al. (2016) suggested that the

secondary compression of soft clay soil occur from the time period of 6-24h for each load increment; summary of loess secondary compression shows that the time corresponding to the demarcation point of primary and secondary compression of loess gradually elapses with the increase in vertical stress and is distributed within 46-200min (Ge et al.2015; Zhi et al. 2018). To reduce the complexity and subjective error of determining the demarcation point, it is considered in this paper that the secondary compression is the period from 200min to deformation stability (the vertical deformation is less than 0.002mm per day). During this time period, the void ratio decreases linearly with the logarithm of time, which slope is defined as the secondary compression index and is usually expressed as $C_a=\Delta e/\log(t_2/t_1)$, where t_1 is the time of demarcation point of primary and secondary compression, t_2 is the time of deformation stability, and Δe is the change in void ratio during the secondary compression stage.

Fig.8 shows the variation of the void ratio with the logarithm of time for loess with different water content, 7.14% (natural water content), 18.03%, 25.10%, and 35.02%(saturated), separately. For all specimens, the void ratio decreases with time at each loading, the rate of change in the void ratio was great high at the beginning of loading, after which it started to decline. Higher volume changes occur in the primary compression stage or secondary compression stage with an increase in vertical stress, particularly for vertical stress more elevated than the yield stress, which is more obvious in the low water content specimens.

Fig.9 compares the variation of void ratio with the logarithm of time for specimens with different water content at similar vertical stresses. It is clear that the rate and magnitude of secondary compression of loess increase with the increase of water content at low vertical stress (Fig.9(a)); however, with the increase of vertical stress, the secondary compression characteristics of loess with different water content tend to be similar. At σ_v=3200kPa, the e-logt curves of each specimen in the secondary compression stage are parallel to each other (Fig.9(d)). It can be concluded that the effect of water content on the secondary compression of loess is gradually weakened with increasing vertical stress. The water softens the cementitious materials in loess (Wen and Yan,2014), and for unsaturated soils, water menisci at the interparticle contacts apply tensile pressure to the skeleton particles for preventing particle rearrangement (Rezania et al.,2020), which lead to the increase of loess secondary compressibility with the increase of water content in low vertical stress. Interparticle cementation and suction hinder the development of secondary compression. For low water content loess, with the increase of vertical stress, the interparticle cementation is gradually destroyed, and the decrease of volume result in an increase in saturation and a decrease in suction, which leads to the secondary compressibility enhanced; for the loess with high water content, it has greater volume change than the loess with low water content at the similar vertical stress, higher density makes the skeleton particles form inter-locking structure, thus slowing down the development of secondary compression.

Fig.10(a) shows the variation curves of the secondary compression index (C_a) with vertical stress for loess with different water contents. It can be seen that the secondary compression index of the low water content loess increases with the increase of vertical stress, and the secondary compression index of higher water content loess increases to the peak and then slightly decreases to constant with the vertical

stress, which is similar to the results of other literature (Perisic et al.,2019; Rezania et al.,2020). Comparing with the compression index curves (Fig.7), it can be found that they show a similar variation pattern in logarithmic of vertical stress. A large number of studies (Mesri,1987; Zhang et al.,2007; Santagata et al.,2008; Carlos,2018) have concluded that C_α/C_c is a constant value independent of stress level and specimen type (Undisturbed or remodeled). However, some studies have found a poor linear correlation between C_α and C_c, Zhang and Wang (2012) speculated that the structure of soft clay prevents its C_α/C_c from a constant value; Mataic et al. (2016) found that the C_α/C_c value of Perniö clay increases with effective stress and then decreases and converges to a constant value (0.036). The C_α/C_c values of the low water content loess firstly increased with the vertical stress to peak and then gradually decreased and stabilized (Fig.10(b)), showing a similar variation pattern as the result of Perniö clay (Mataic et al.2016). However, a little different is that the C_α/C_c values of the higher water content loess gradually decreased and tended to stabilize, and did not show a peak, the C_α/C_c values of all specimens converged to around 0.025 eventually.

Microstructure analyses

Microstructure of intact and saturated loess

This section describes the microstructure of intact and saturated loess in terms of four elements: particle pattern、contact relation、bonding material、pore size distribution, to illustrate the effect of water content on the microstructure of loess and to provide a basis for further analyzing the effect on compressibility.

Fig.11(a), (b) is the SEM images of intact loess, where the overall microstructure such as skeletal particles and pore distribution are observed in the low magnification image, and the surface morphology of the particles, interparticle contact, and bonding material are observed in the high magnification image. In addition to silt and sand, aggregates are also an essential part of skeleton particles in intact loess, which are formed when a large number of clay particles clumped together on their own or when clay particles and carbonates bind the silt and sand (Gao,1980; Li et al.,2016; Liu et al.,2016; Pihlap et al.,2021). In the deposition, the skeleton particles are randomly and loosely arranged, making the loess form an opening metastable structure. Lanzhou intact loess has the typical microstructure characteristics of loess: silt, sand, and aggregates are contacted point-to-point, and there are only a few bonds at the contact, forming an overhead pore structure (Fig.11(a)). The cementation of clay and calcium carbonate in loess plays a vital role in the metastable structure (Cliek,2001; Smalley and Marković,2014; Li et al.,2016; Liu et al.,2016; Yates et al.,2017; Meng and Li.,2019), Fig.11(b) clearly shows that clay particles are distributed on the surface and contact point of skeleton particles and do not exist alone. Secondary calcium carbonate can occur due to the precipitation of carbonates (Pihlap et al.,2021), which reinforce the bonding structure and help to trap clay particles at skeleton particles contacts (Smalley and Marković, 2014). Although it is difficult to observe the secondary calcium carbonate directly, some experiments show that the strength of the loess decrease obviously after removing the calcium carbonate, which can also prove the cementation of the secondary calcium carbonate (Meng and Li, 2019). The high compressibility of intact loess and its sensitivity to water mainly comes from the overhead pore structure

and the softening effect of water on cementation materials, where the high porosity provides space for compression deformation, and the hydrophilicity of clay minerals makes the compressibility of loess extremely sensitive to the change of water content. The microstructure of saturated loess shows in Fig.11(c), (d), which is still dominated by overhead pore structure, but compared with intact loess, the distribution of skeleton particles and pores is more uniform, and the macropores are closed. The most significant phenomenon is the disappearance of the aggregates prevalent in the intact loess after saturation.

Mercury intrusion porosimetry (MIP) has been proved to be one of the reliable methods to measure pore distribution of soil, which has been widely used in loess (Ng et al.,2016; Wang et al.,2018). Lei (1987) divided pores of loess into four types according to the pore radius: large pores (>16μm), mediate pores(4-16μm), small pores(1-4μm) and micropores(<1μm), which is referred to in this paper. Fig12 shows the cumulative pore volume curves and pore distribution curves of intact loess and saturated loess. There are two peaks in the intact loess and saturated loess pore distribution curves (PSDs), indicating two major pore groups in the loess structure. The first pore group with a dominant mediate pore diameter is about 9.7μm for intact loess and about 8.3μm for saturated loess, and the second pore group with a small pore has a nearly identical diameter of about 3.5μm for intact and saturated loess, which indicate that pore size decreases slightly after saturation. The effect of saturation on the pore structure of loess is significant in the pore volume. The cumulative intrusion pore volume of intact loess with 0.28 decreases to 0.23 after saturating, indicating self-weight collapse due to inundating. On the other hand, in intact loess mediate pore accounts for 69.38% of the total pore volume and decreases to 41.31% after saturation, and small pores increase from 15.67% to 35.33%; therefore, it can be seen that mediate pore collapsed when the loess was inundated, leading to the transformation from mediate pores to small pores. In terms of total pore volume and pore size, inundation reconstructs the pore structure of loess, makes it more homogeneous, and causing some damage to the original microstructure of the intact loess.

Microstructure of loess with different water content after compression

The compression tests show that the water content has a significant influence on the compressibility of the loess, and the damage of hydraulic effect on loess microstructure is also analyzed. However, to reveal the evolution of loess compressibility under wetting and loading through the change of loess microstructure under hydro-mechanical effect, it is necessary to understand the microstructure changes of loess with different moisture content after compression. Therefore, three post-compression samples of loess with different water content are selected for SEM and MIP, which are 7.14% (natural state), 18.03% (saturation 50.03%), and 35.03% (saturated state).

Fig.13 shows the microscopic images of the loess with different water content after compression, which can be seen that the microstructure of saturated loess is subject to drastically change compared to others. For intact loess (Fig.13a, b), aggregates and intergranular cementation are destroyed under load, overhead structures collapse, the intergranular pores become small, and part of which is filled with clay

particles, and the skeleton particles contact more closely. However, it is still dominated by the point-to-point and point-to-face contact of skeleton particles and retains some microstructure characteristics of undisturbed loess. Comparison between the microscopic images of the sample with natural water content (Fig.13a) and the microscopic images of samples with higher water content (Fig.13c, e) suggests that the microstructure is closer and homogeneous as the water content is increased. From details (comparison Fig.13b and Fig.13d, f), the microstructure changes from overhead structure to interlocking structure with the water content are increased. It can be summarized by the fact that the microstructure of loess has undergone a radical transformation under the action of saturating and loading; in terms of microstructure, even after compression with high stress, the intact loess still retains some original structure and has the potential to compress further under higher loads or inundation.

Fig.14 shows the pore size distribution curves of the loess with different water content after compression. Compared to the cumulative intruded pore volume of the intact loess (Fig.12), compression leads to a significant reduction in the total pore volume of the loess, and the reduction in pore volume decreases more with increasing water content. The pore size distribution curves of the compressed specimens show a more significant change from a bimodal peak to a single peak compared to the undisturbed loess specimen, regardless of the water content. This is because the mediate pores collapse to the small pores during the compression process, which is reflected in the pore size distribution curve as the bimodal peak of the PSD is eliminated and transformed into a single peak. Moreover, in response to an increase in water content, the height of single peak decreases, and the peak that defines the dominant pore diameter on the PSD shifts to the left. In other words, compression with high pressure can not eliminate the collapsible pores of intact loess, and wetting can promote the further collapse of mediate pores to form a more compact structure.

The evolution of microstructure and pore distribution due to wetting and loading is consistent with the compression responses of intact loess. Under low vertical stress, microstructure damage due to wetting is one of the key factors for the great difference of compressibility of loess; Under high vertical stress, the intact loess still retains some original microstructure and pore space, but microstructure damage is aggravated to form a compact interlocking structure due to wetting.

Conclusions

A series of oedometer tests were performed to determine the compression characteristics of intact loess with different water contents. SEM and MIP tests were also carried out on specimens before and after compression to understand the evolution of microstructure and pore size distribution during wetting and loading. The following conclusions can be drawn:

For intact loess, the increase of water content results in an increase in the slope of the compression curve and the values of secondary compression index, and a decrease in yield stress. The C_c and C_α increase with the vertical stress, for intact loess with low initial water content, the C_c values are very small and increase suddenly after exceeding the yield stress; for intact loess with high initial water content, the C_c

values and its change rate are relatively large, but the change gradually slows down with the vertical stress; C_α shows a similar variation pattern in logarithmic of vertical stress as the compression index. The C_α/C_c value of intact loess dependent on the water content and the vertical stress and cannot be considered a constant value; however, it tends to a constant value of about 0.025 under high vertical stress.

The intact loess has a loose arrangement of silt and aggregates, weakly cemented overhead structure, and bimodal pore distribution dominated by mediate and small pores. Inundating leads to the collapse of aggregates and overhead structure, uniform particle distribution, reduction of mediate pores, and transformation into small pores. After compression, the overhead structure of the intact loess collapses, the pore volume decreases, the bimodal peak of PSD is eliminated and transformed into a single peak. Compression with high pressure can not drastically eliminate the collapsible pores of intact loess, and wetting can further collapse mediate pores to form a more compact structure.

Declarations

Acknowledgments

This work was supported by the National Key R&D Program of China (Grant No. 2018YFC 1505304) and the National Natural Science Foundation of China (No. 41877281, 41772339).

References

1. Assallay A M, Rogers C D F, Smally I J (1997) Formation and collapse of metastable particle packings and open structures in loess deposits. Eng Geol 48:101-115.
2. Bally R J (1988) Some specific problems of wetted loessial soils in civil engineering. Eng Geol 25(2-4):303-324.
3. Barden L, Mcgown A, Collins K (1973) The collapse mechanism in partly saturated soil. Eng Geol 7(1):49-60.
4. Benatti J C B, Miguel M G (2013) A proposal of structural models for colluvial and lateritic soil profile from southwestern Brazil on the basis of their collapsible behavior. Eng Geol 153:1-11.
5. Carlos O (2018) On the role of particle breakage in primary and secondary compression of wet and dry sand[J]. Geotech Lett 8(2):1-15.
6. Chen C L, Hu Z Q, Gao P (2006) Research on relationship between structure and deformation property of intact loess. Chin J Rock and Soil Mech 11:1891-1896((**In Chinese**))
7. Cheng Q, Zhou C, Ng C W W, et al (2020) Effects of soil structure on thermal softening of yield stress. Eng Geol 269:105544.
8. Cilek V (2001) The loess deposits of the Bohemian Massif: silt provenance, palaeometeorology and loessification processes. Quatern Int 77:123-128.

9. Dijkstra T A, Smalley I J, Rogers C D F (1995) Particle packing in loess deposits and the problem of structure collapse and hydroconsolidation. Eng Geol 40:49-64.
10. Francisca, Franco M (2007) Evaluating the Constrained Modulus and Collapsibility of Loess from Standard Penetration Test. Int J Geomech 7(4):307-310.
11. Gao G R (1980a) The microstructure of loess in China. Chin Sci Bull 20: 945-948((**In Chinese**))
12. Gao G R (1980b) Classification for microstructure of loess and its collapsibility. Sci Sin, 12:1203-1208((**In Chinese**))
13. Gao G R (1988) Formation and development of the structure of collapsing loess in China. Eng Geol 25(2-4):235-245.
14. Ge M M, Li N, Zheng J G, et al (2015) Prediction of the post-construction settlement of high filled embankment with considering the time depending deformation of compacted loess[J]. Chin Civil Eng J 48(S2):262-267 ((**In Chinese**))
15. Gibbs H J, Holland W Y (1960) Petrographic and engineering properties of loess, US Bureau of Reclamation. Eng. Monogr. 28,37.
16. Grabowska-Olszewska B (1989) Skeletal microstructure of loesses-its significance for engineering-geological and geotechnical studies. Appl Clay Sci 4(4):327-336.
17. Handy R L (1973) Collapsible Loess in Iowa. Soil Sci Soc Am J 37(2): 281-284.
18. Hou X K, Vanapalli S K, Li T L (2018) Water infiltration characteristics in loess associated with irrigation activities and its influence on the slope stability in Heifangtai loess highland, China. Eng Geol 234:27-37.
19. Hou X K, Vanapalli S K, Li T L (2019) Wetting-induced collapse behavior associated with infiltration: A case study. Eng Geol 258:105146.
20. Jiang M J, Hu H J, Liu F (2012) Summary of collapsible behaviour of artificially structured loess in oedometer and triaxial wetting tests. Can Geotech J 49(10): 1147-1157.
21. Jiang M J, Zhang F G, Hu H J, et al (2014) Structural characterization of natural loess and remolded loess under triaxial tests. Eng Geol 181:249-260.
22. Juang C H, Dijkstra T, Wasowski J, et al (2019) Loess geohazards research in China: Advances and challenges for mega engineering projects. Eng Geol 251:1-10.
23. Lei X Y (1987) Pore types of the loess in China and its collapsibility. Sci Sin 12:1309-1318((**In Chinese**))
24. Leng Y Q, Peng J B, Wang Q Y, et al (2018) A fluidized landslide occurred in the Loess Plateau: A study on loess landslide in South Jingyang tableland. Eng Geol 236:129-136.
25. Leng Y Q, Peng J B, Wang S, et al (2021) Development of water sensitivity index of loess from its mechanical properties. Eng Geol 280(3):105918.
26. Li P, Shao S J, Vanapalli S K (2020) Characterizing and modeling the pore-size distribution evolution of a compacted loess during consolidation and shearing. J Soil Sediment 20(7) 2855-2867.

27. Li P, Vanapalli S, Li T L (2016) Review of collapse triggering mechanism of collapsible soils due to wetting. J Rock Mech Geotech 8(02):256-274.
28. Li X A, Li L C (2017) Quantification of the pore structures of Malan loess and the effects on loess permeability and environmental significance, Shaanxi Province, China: an experimental study. Environ Earth Sci 76(15):523.
29. Li X A, Li L, Song Y X, et al (2019) Characterization of the mechanisms underlying loess collapsibility for land-creation project in Shaanxi Province, China—a study from a micro perspective. Eng Geol 249:77-88.
30. Liu T S (1985) Loess and environment. Science Press, Beijing, pp1-481 ((**In Chinese**))
31. Liu Z, Liu F Y, Ma F L, et al (2016) Collapsibility, composition, and microstructure of loess in China. Can Geotech J 53:673-686.
32. Lu Q Z, Qiao J W, Peng J B, et al (2019) A typical Earth fissure resulting from loess collapse on the loess plateau in the Weihe Basin, China. Eng Geol 259:105189.
33. Mataic I, Wang D X, Korkiala-Tanttu L (2016) Effect of destructuration on the compressibility of Pernio Clay in incremental loading oedometer tests. Int J Geomech 16(1):040150161.
34. Meng J, Li X A (2019) Effects of carbonate on the structure and properties of loess and the corresponding mechanism: an experimental study of the Malan loess, Xi'an area, China. Bull Eng Geol Environ 78(7):4965-4976.
35. Mesri G, Castro A (1987) C_a/C_c concept and K_0 during secondary compression. Int J Geotech Geo 113: 230-247.
36. Mitchell J K, Soga K (2005) Fundamentals of soil behaviour,3rd ed. John Wiley & Sons, New Jersey, pp:353-355.
37. Munoz-Castelblanco J A, Delage P, Pereira J M, et al (2012) On-sample water content measurement for a complete local monitoring in triaxial testing of unsaturated soils. Géotechnique 62(7): 595-604.
38. Ng C W W, Sadeghi H, Hossen S B, et al (2016) Water retention and volumetric characteristics of intact and re-compacted loess. Can Geotech J 53:1258-1269.
39. Nouaouria M S, Guenfoud M, Lafifi B (2008) Engineering properties of loess in Algeria. Eng Geol 99(1-2):85-90.
40. Perisic G A, Ovalle C, Barrios A (2019) Compressibility and creep of a diatomaceous soil[J]. Eng Geol 258:105145.
41. Pihlap E, Steffens M, Kgel-Knabner I (2021) Initial soil aggregate formation and stabilisation in soils developed from calcareous loess. Geoderma 385:114854.
42. Rezania M, Bagheri M, Nezhad M M (2020) Creep and consolidation of a stiff clay under saturated and unsaturated conditions[J]. Can Geotech J 57:728-741.
43. Reznik Y M (1992) Determination of deformation properties of collapsible soils. Geotech Test J 15(3):248-255.

44. Sadeghi H, Kiani M, Sadeghi M, et al (2019) Geotechnical characterization and collapsibility of a natural dispersive loess. Eng Geol 250:89-100.
45. Santagata M, Bobet A, Johnston C T, et al (2008) One-dimensional compression behavior of a soil with high organic matter content. J Geotech Geoenviron Eng 134(1):1-13.
46. Saye S R, Nass K H, Easton C N (1988) Performance of heavy structures founded upon loess at varying moisture conditions. Eng Geol 25(2-4):325-339.
47. Shao S J, Li J, Li G L, et al (2015) Evaluation method for self-weight collapsible deformation of large thickness loess foundation. Chin J Geotech Eng (06):965-978((**In Chinese**))
48. Shao X X, Zhang H Y, Tan Y (2018) Collapse behavior and microstructural alteration of remolded loess under graded wetting tests. Eng Geol 233:11-22.
49. Smalley I J, Marković S B (2014) Loessification and hydroconsolidation: There is a connection. Catena 117:94-99.
50. Sridharan A, Abraham B M, Jose B T (1991) Improved technique for estimation of preconsolidation pressure. Géotechnique 41(2):263-268.
51. Standardization Administration of China (SAC), Ministry of Water Resources (2019) China National Standards GB/T50123-2019: Standard for Soil Test Method. China Planning Press, Beijing ((**In Chinese**))
52. Wang J D, Li P, Ma Y, Vanapalli S K (2018) Evolution of pore-size distribution of intact loess and remolded loess due to consolidation. J Soil Sediment 19(3):1226-1238.
53. Wang J D, Li P, Ma Y, et al (2020a) Change in pore-size distribution of collapsible loess due to loading and inundating[J]. Acta Geotech 15(5):1081-1094.
54. Wang L Q, Shao S J, She F T (2020b) A new method for evaluating loess collapsibility and its application. Eng Geol 264:105376.
55. Wen B P, Yan Y J (2014) Influence of structure on shear characteristics of the unsaturated loess in Lanzhou, China. Eng Geol 168:46-58.
56. Xie D Y, Xing Y C (2016) Soil mechanics for loess soils. Higher Education Press, Beijing pp:37-50 ((**In Chinese**))
57. Xie W L, Li P, Vanapalli S K, Wang J D (2018) Prediction of the wetting-induced collapse behaviour using the soil-water characteristic curve. J Asian Earth Sci 151:259-268.
58. Xu L, Dai F C, Tu X B, et al (2014) Landslides in a loess platform, North-West China. Landslides 11(6):993-1005.
59. Yang Y S, Li J, Xing Y C, et al (2017) Experimental study on moistening deformation characteristics of compacted loess and their influencing factors. Chin J Geotech Eng 39(04):626-635((**In Chinese**))
60. Yates K, Fenton C H, Bell D H (2018) A review of the geotechnical characteristics of loess and loess-derived soils from Canterbury, South Island, New Zealand. Eng Geol 236: 11-21.
61. Youssef A M, Maerz N H (2013) Overview of some geological hazards in the Saudi Arabia. Environ Earth Sci 70(7):3115-3130.

62. Zhang W B, Xie Y L, Yang X H (2007) Research on 1D secondary consolidation characteristics of compacted loess. Chin J Geotech Eng 29(05):765-768 ((**In Chinese**))
63. Zhang W P, Sun Y F, Chen W W, et al (2019) Collapsibility, composition, and microfabric of the coastal zone loess around the Bohai Sea, China. Eng Geol 257:105142.
64. Zhang X W, Wang C M (2012) Effect of soft clay structure on secondary consolidation coefficient. Chin J Rock and Soil Mech 33(02):479-482 ((**In Chinese**))
65. Zhi B, Wang P, Wang Y X, et al (2018) Study on properties of secondary consolidation of structured loess under high fill. Chin J Eng Geol 26(6):1447-1453((**In Chinese**))

Tables

Table 1. Geotechnical characteristics of the studied loess.

Property	Value
Sample depth: m	3-4
Natural water content w: %	7.14
Natural degree of saturation S_r: %	20
Specific gravity G_s	2.78
Dry unit mass ρ_d: g/cm^3	1.396
Clay fraction(<5μm): %	10.36
Silt fraction(5μm~75μm): %	80.78
Sand fraction(>75μm): %	8.86
Plastic limit w_p: %	17.9
Liquid limit w_l: %	29.7
Plasticity index I_p	11.8
Main minerals	
Quartz: %	46.31
Albite: %	19.20
Calcite: %	13.23
Illite: %	14.12
Clinochlore: %	5.42
Dolomite: %	1.72

Table 2. Specimens of oedometer test

Test	Sample description	Initial state				Final state			
		e_0	ρ_{d0}(g/cm^3)	w_0(%)	S_{r0}(%)	e_f	ρ_{df}(g/cm^3)	w_f(%)	S_{rf}(%)
SL01	Natural state	0.992	1.396	7.14	20.01	0.749	1.589	7.03	26.09
SL02	Wetting	0.990	1.397	10.45	29.34	0.694	1.641	9.32	41.34
SL03	Wetting	0.992	1.396	13.91	38.97	0.648	1.687	11.76	59.03
SL04	Wetting	0.993	1.395	18.03	50.08	0.629	1.706	13.15	75.80
SL05	Wetting	0.987	1.399	21.19	59.68	0.624	1.712	17.34	77.25
SL06	Wetting	0.991	1.396	25.10	70.22	0.593	1.745	18.33	85.93
SL07	Wetting	0.993	1.395	28.64	80.17	0.576	1.764	18.84	90.93
SL08	Wetting	0.991	1.396	32.08	89.85	0.558	1.784	18.91	96.20
SL09	Vacuum saturation	0.993	1.395	35.02	98.03	0.532	1.815	18.98	99.18

Figures

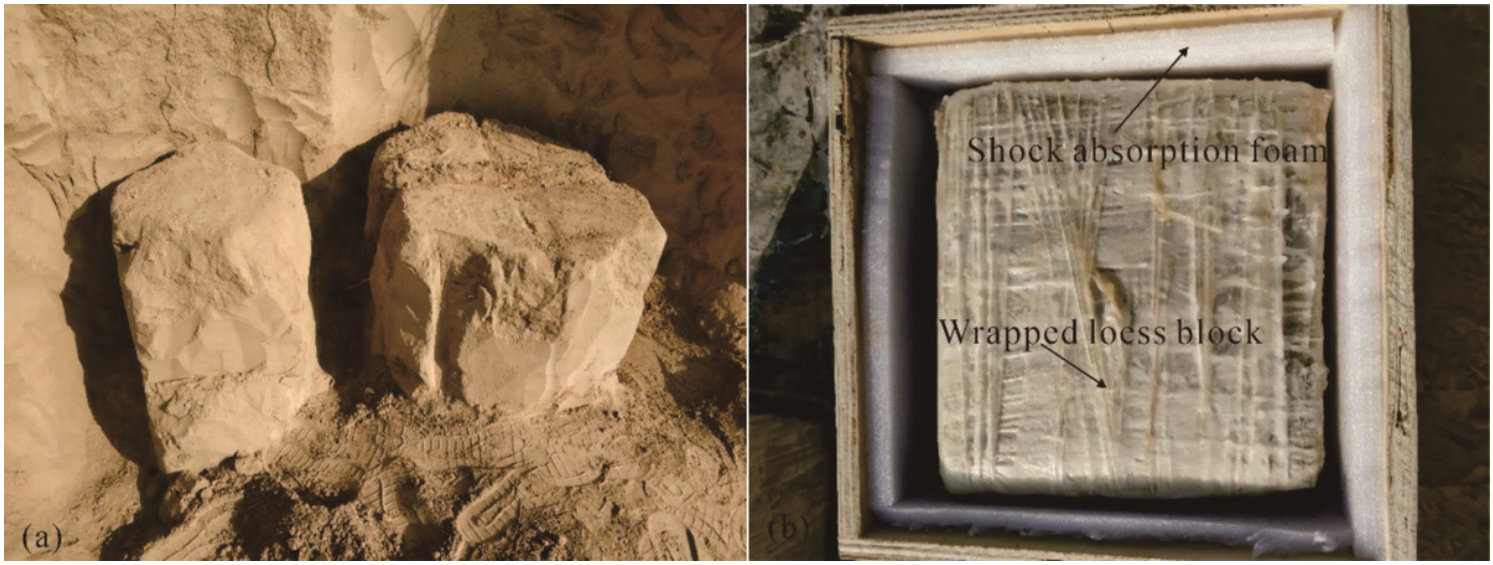

Figure 1

Procedures of block sampling: (a)trimming a block sample; (b)Packing with a plastic membrane and preserving the sample in a wooden box.

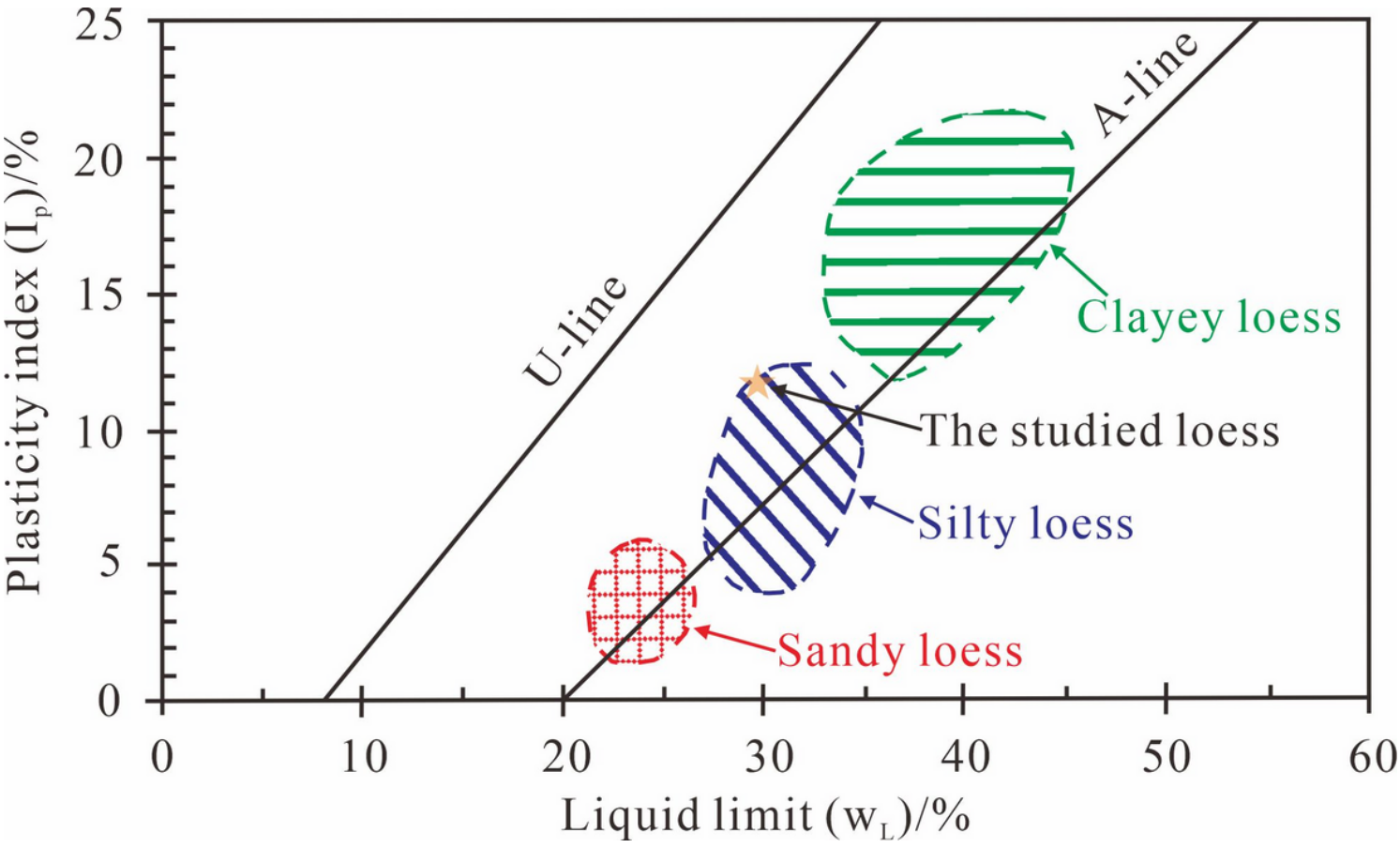

Figure 2

Plasticity chart shows the loesses' classification (Gibbs and Holland,1960).

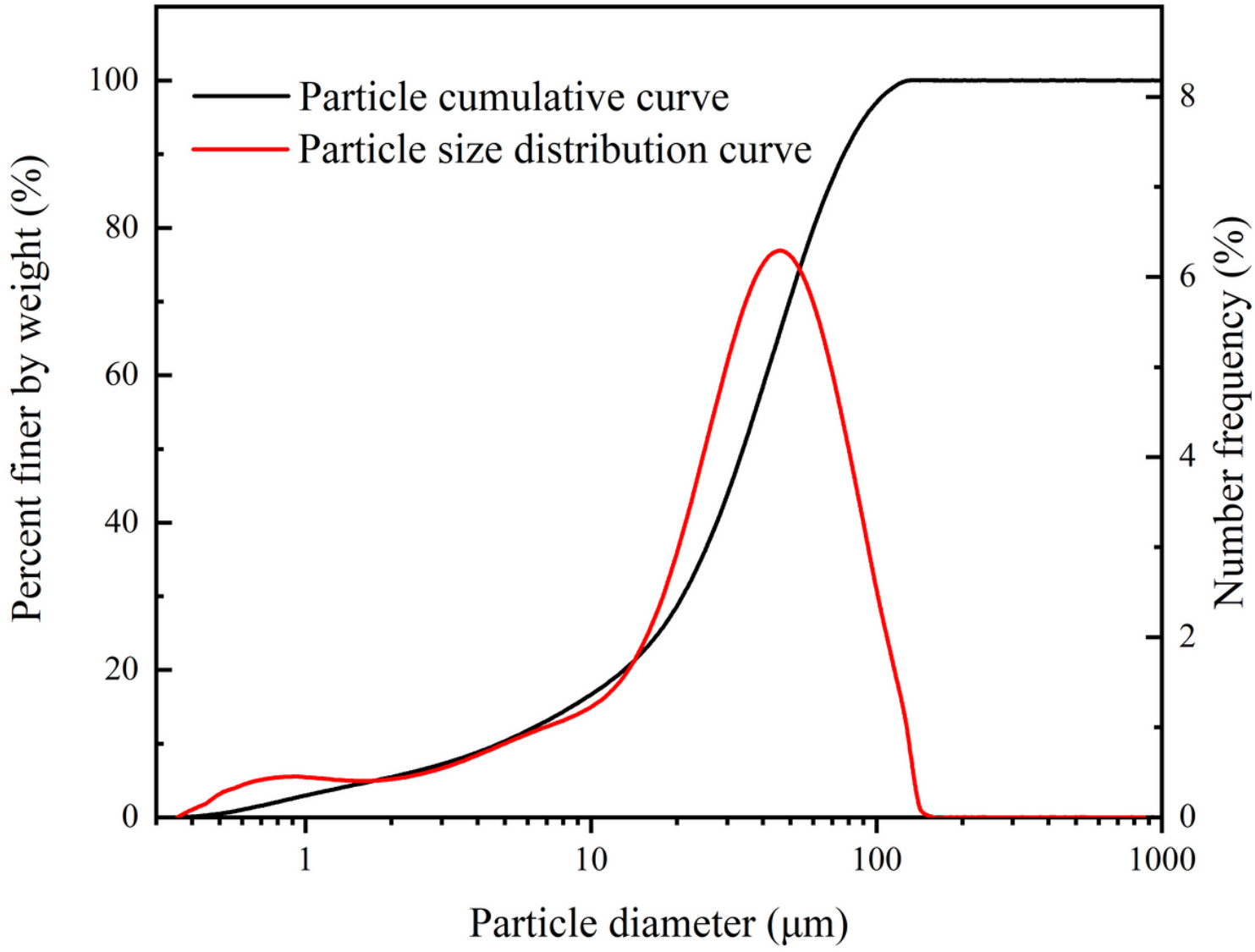

Figure 3

Particle size distribution of studied loess.

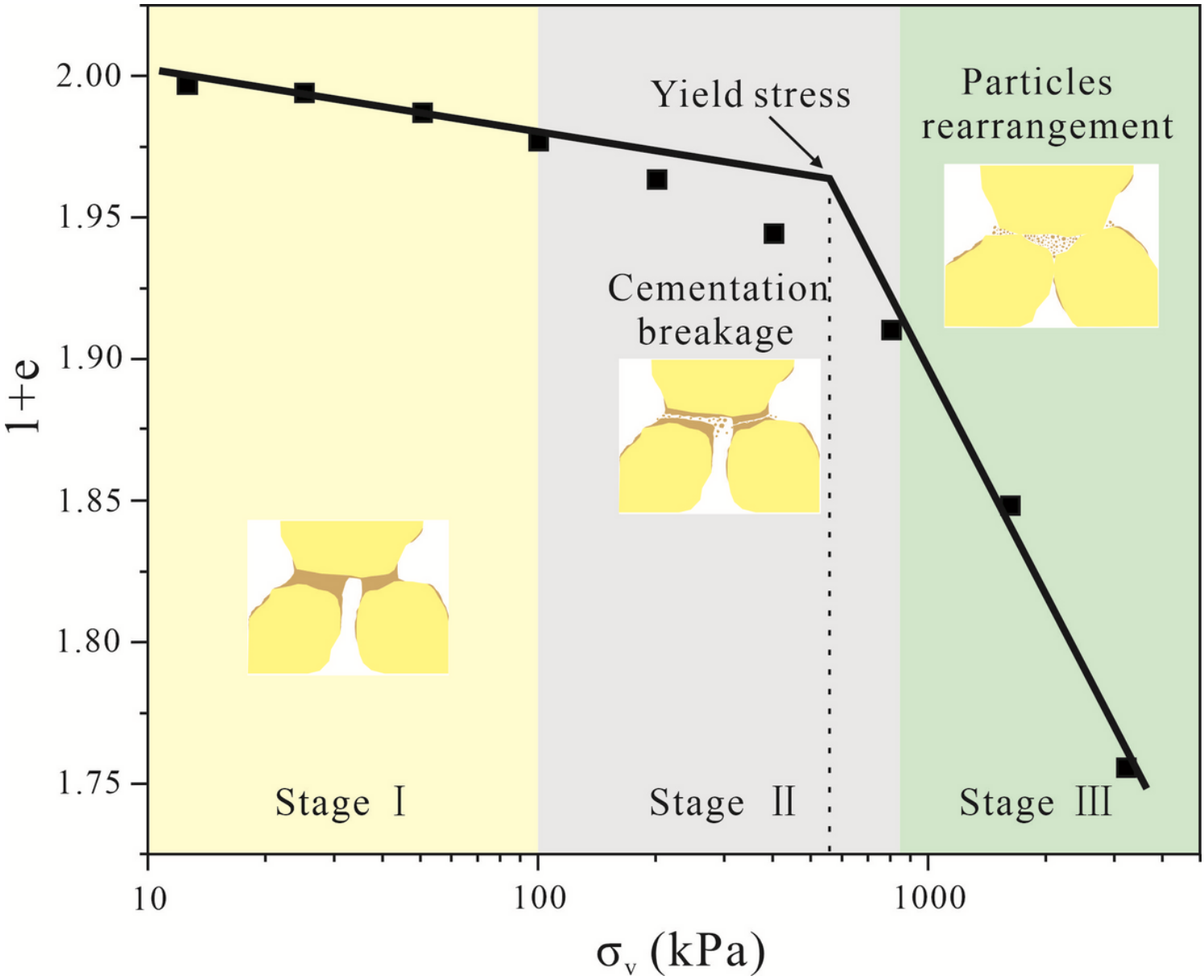

Figure 4

Schematic diagram of loess compression evolution process.

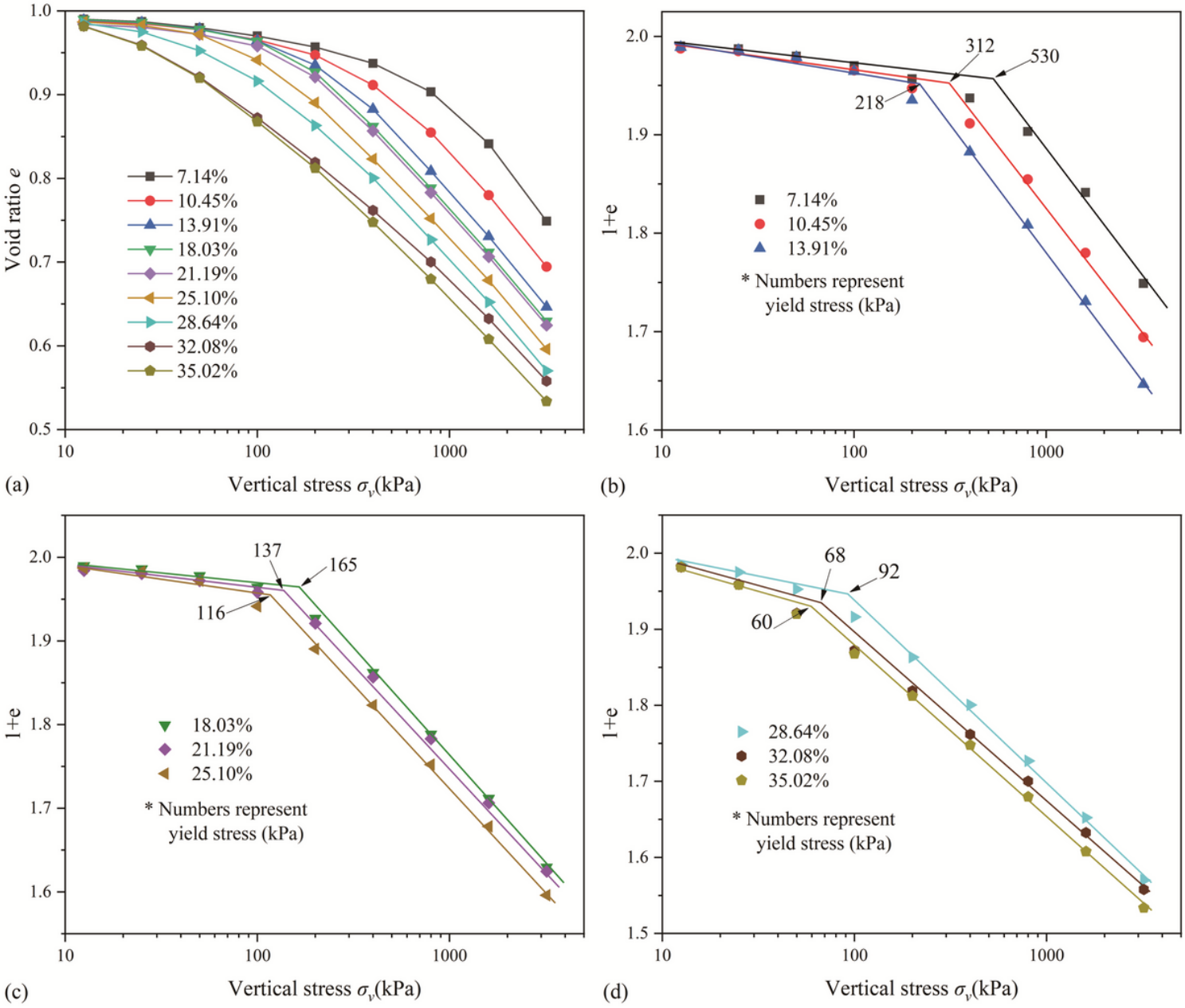

Figure 5

Compression curve of intact loess with different water content:(a) compression curves in an e-logσ_v coordinate system;(b), (c), (d)compression curves in an ln(1+e)-logσ_v coordinate system.

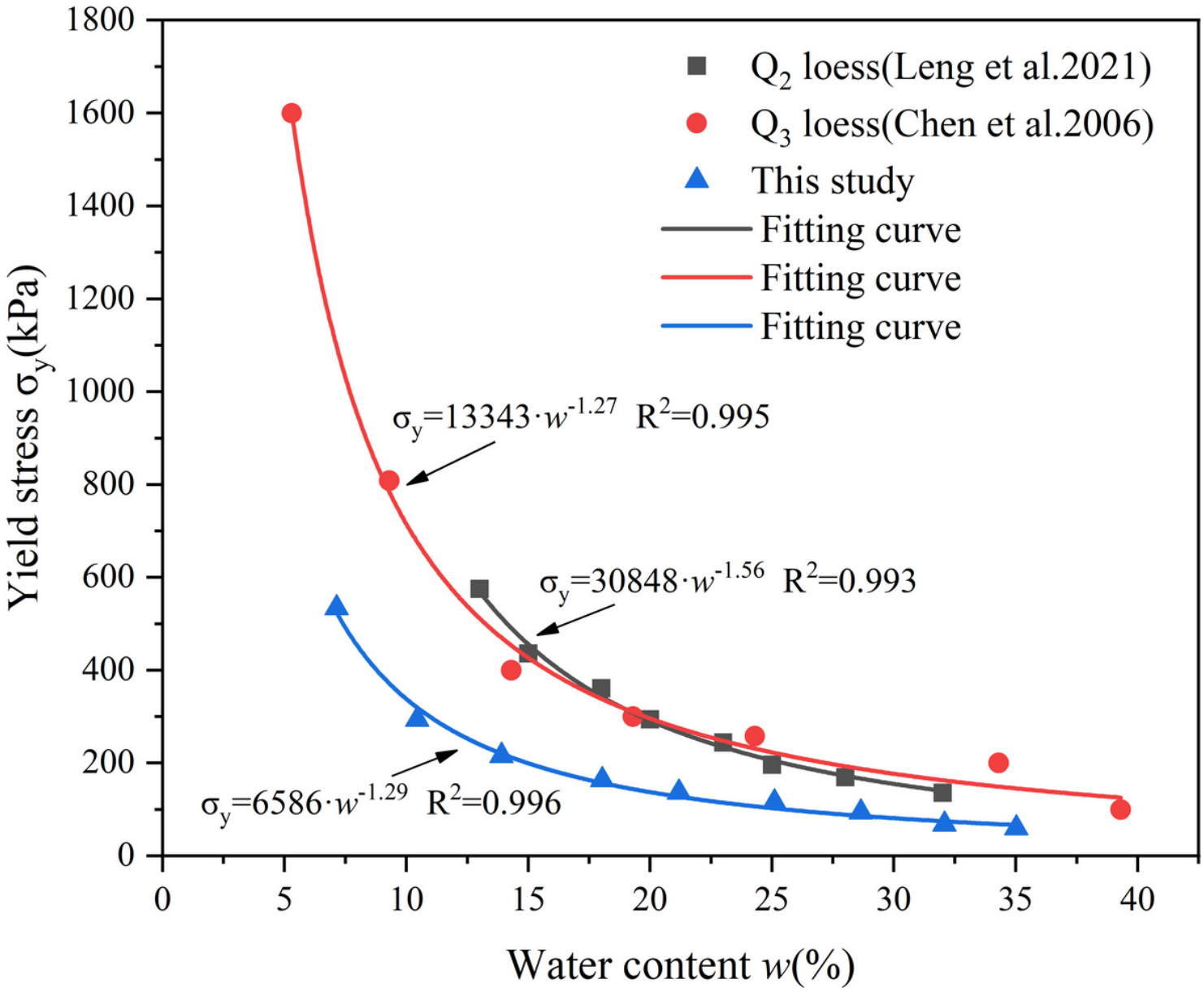

Figure 6

Relationships between yield stress and water content of intact loess.

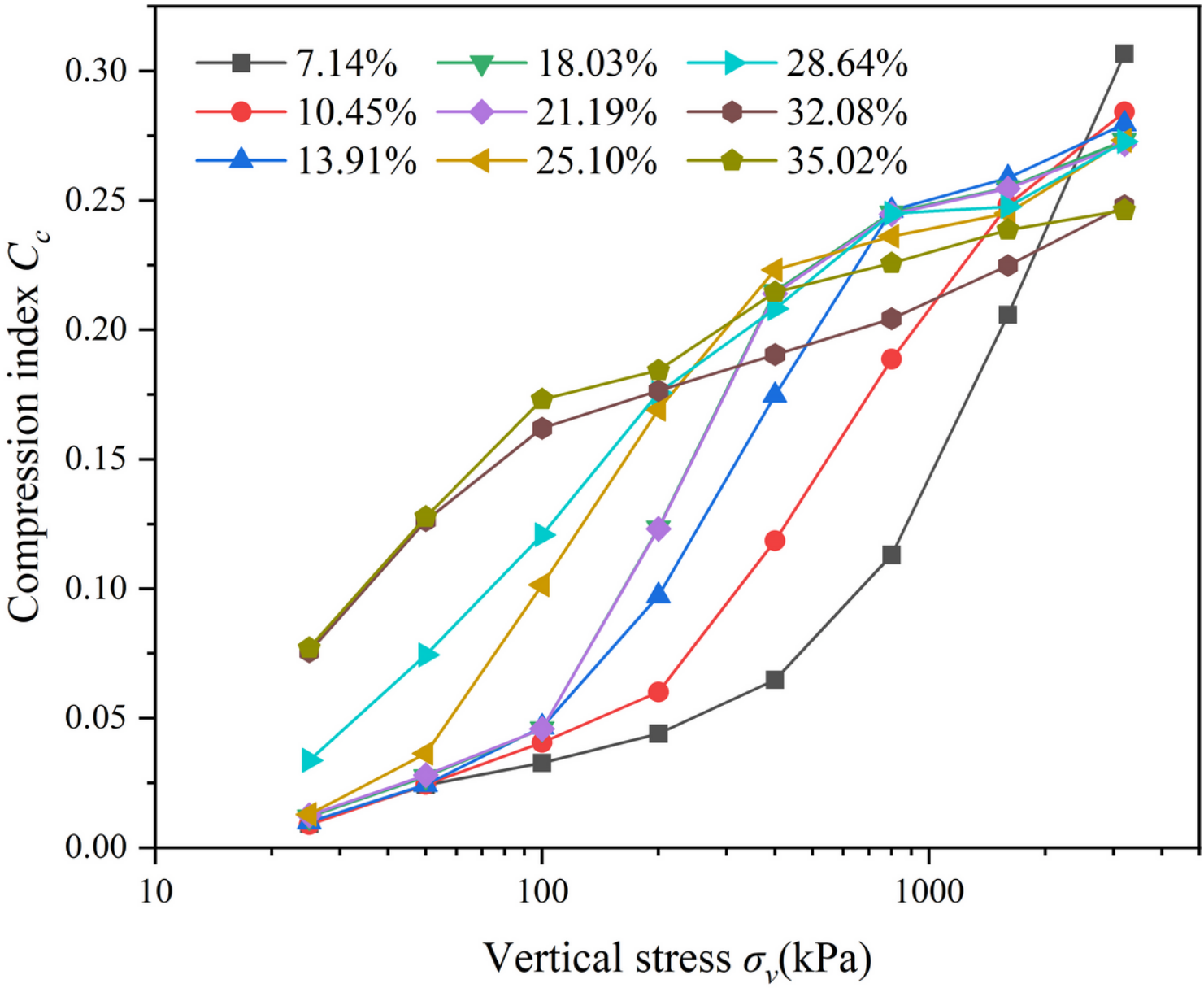

Figure 7

Variation of compression index C_c with vertical stress for intact loess with different water content.

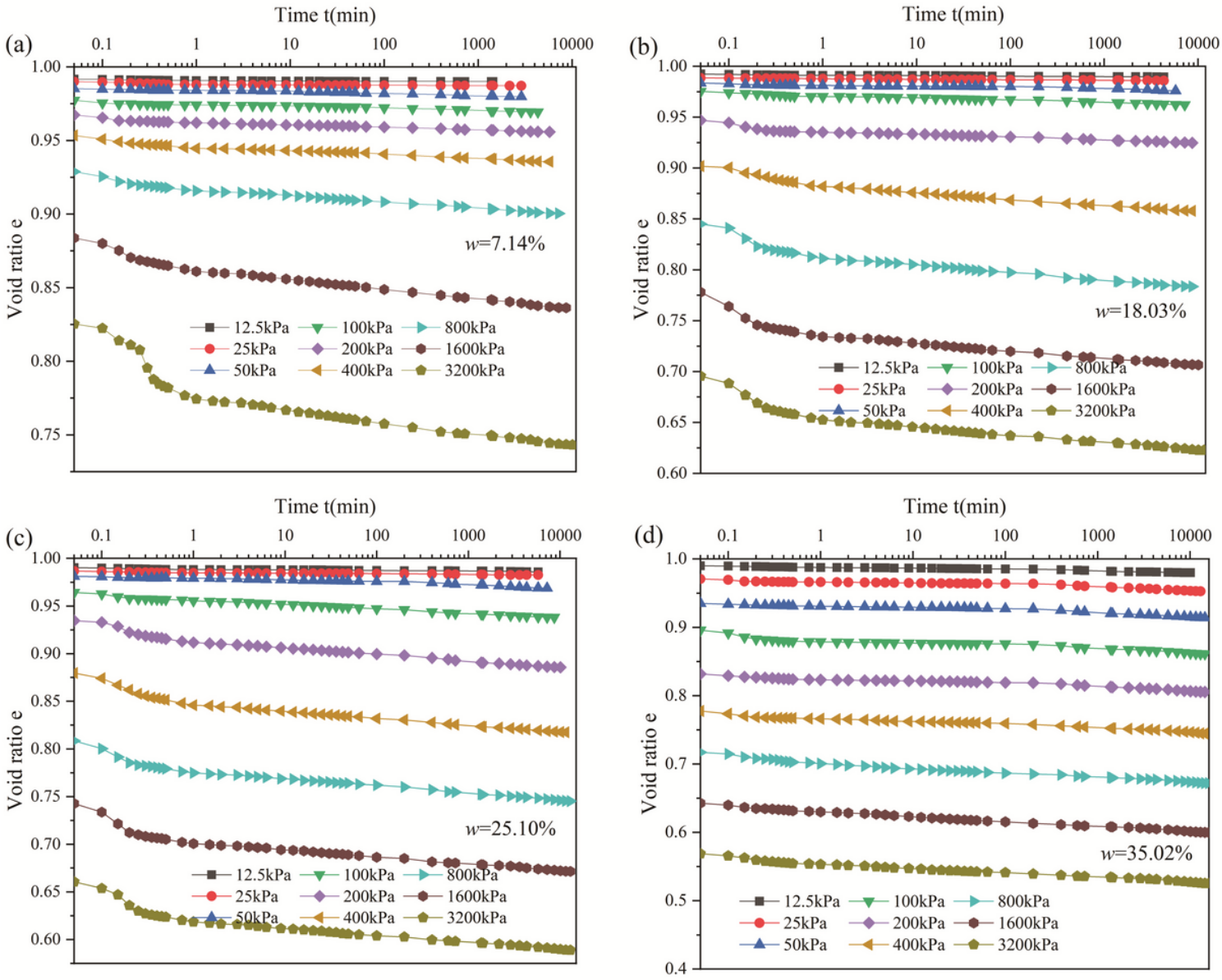

Figure 8

Variation of void ratio with time for intact loess: (a) w=7.14%, (b) w=18.03%, (c) w=25.10%, (d) w=35.02%.

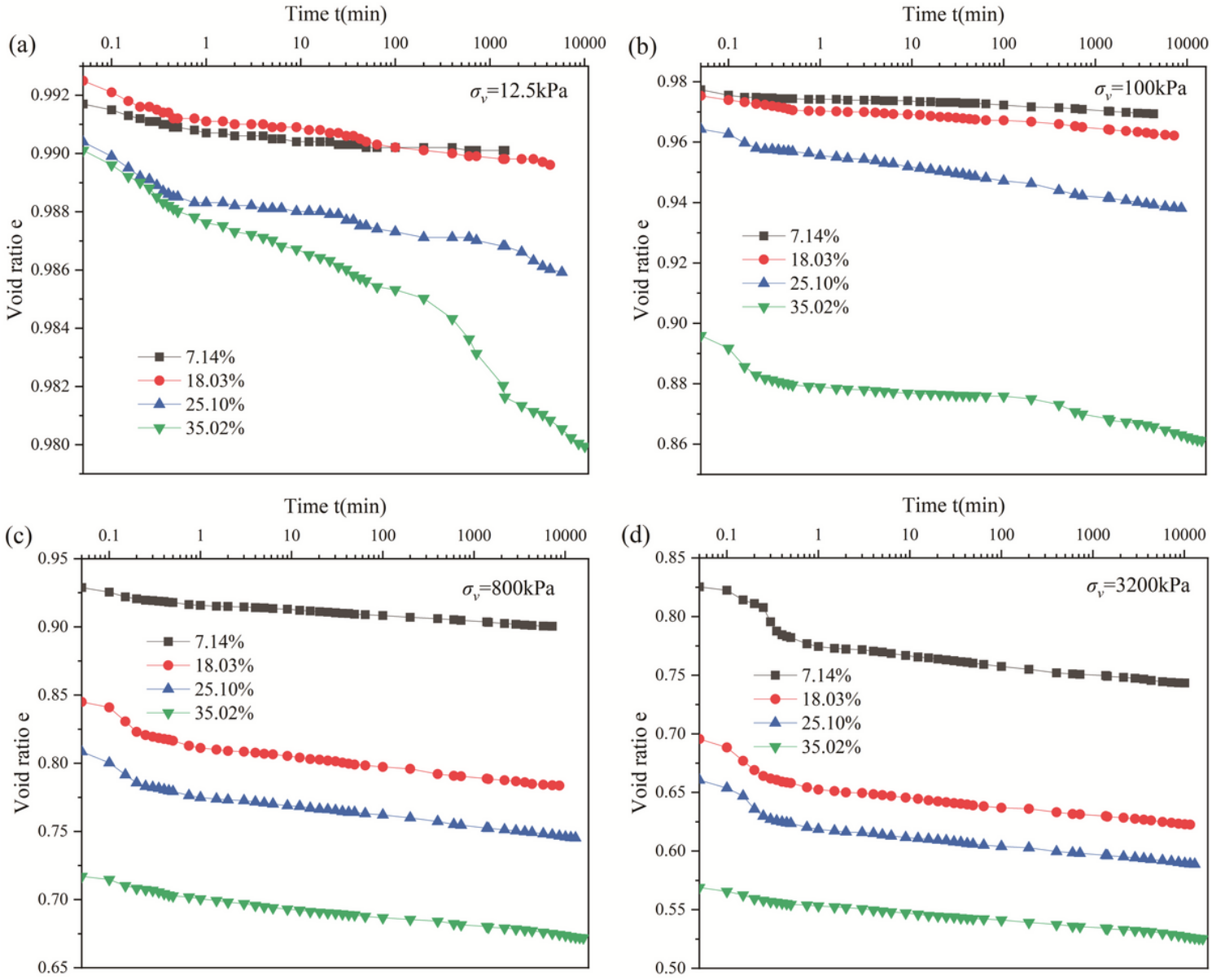

Figure 9

Variation of void ratio with time for intact loess with different water content: (a) 12.5kPa, (b)100kPa, (c)800kPa, (d)3200kPa.

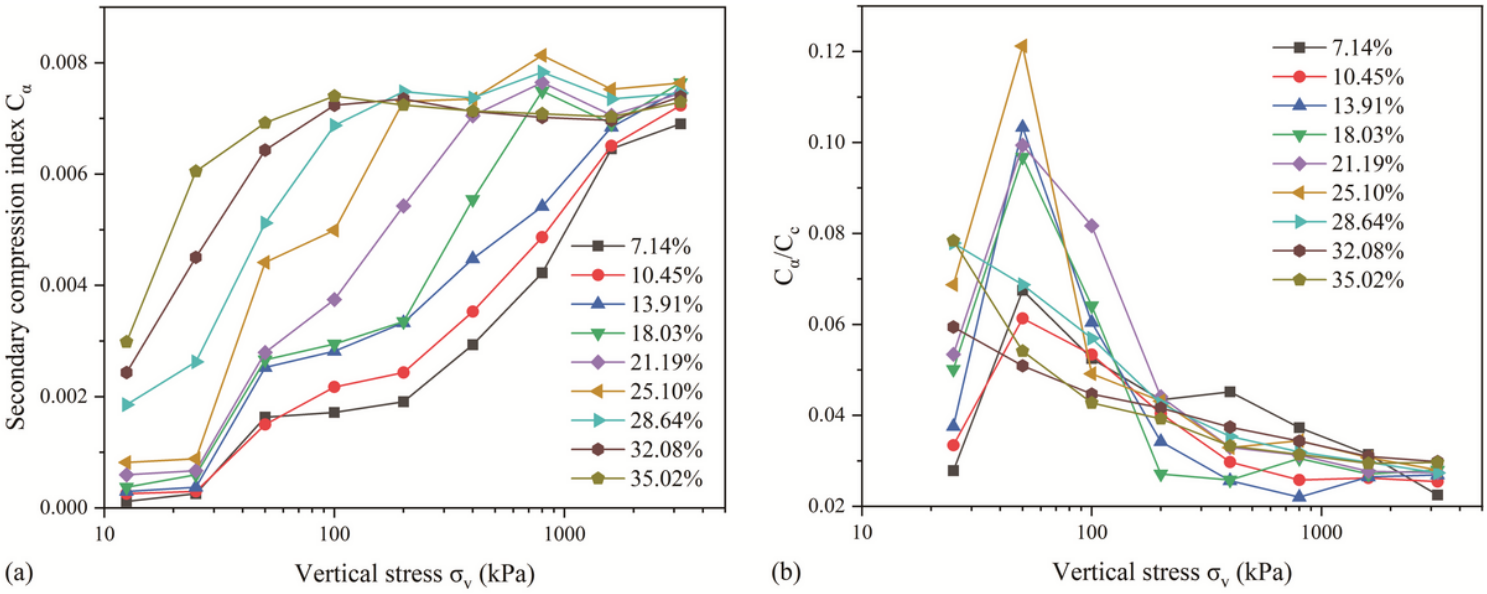

Figure 10

Variation of secondary compression index C_c and C_α/C_c with vertical stress for intact loess with different water content.

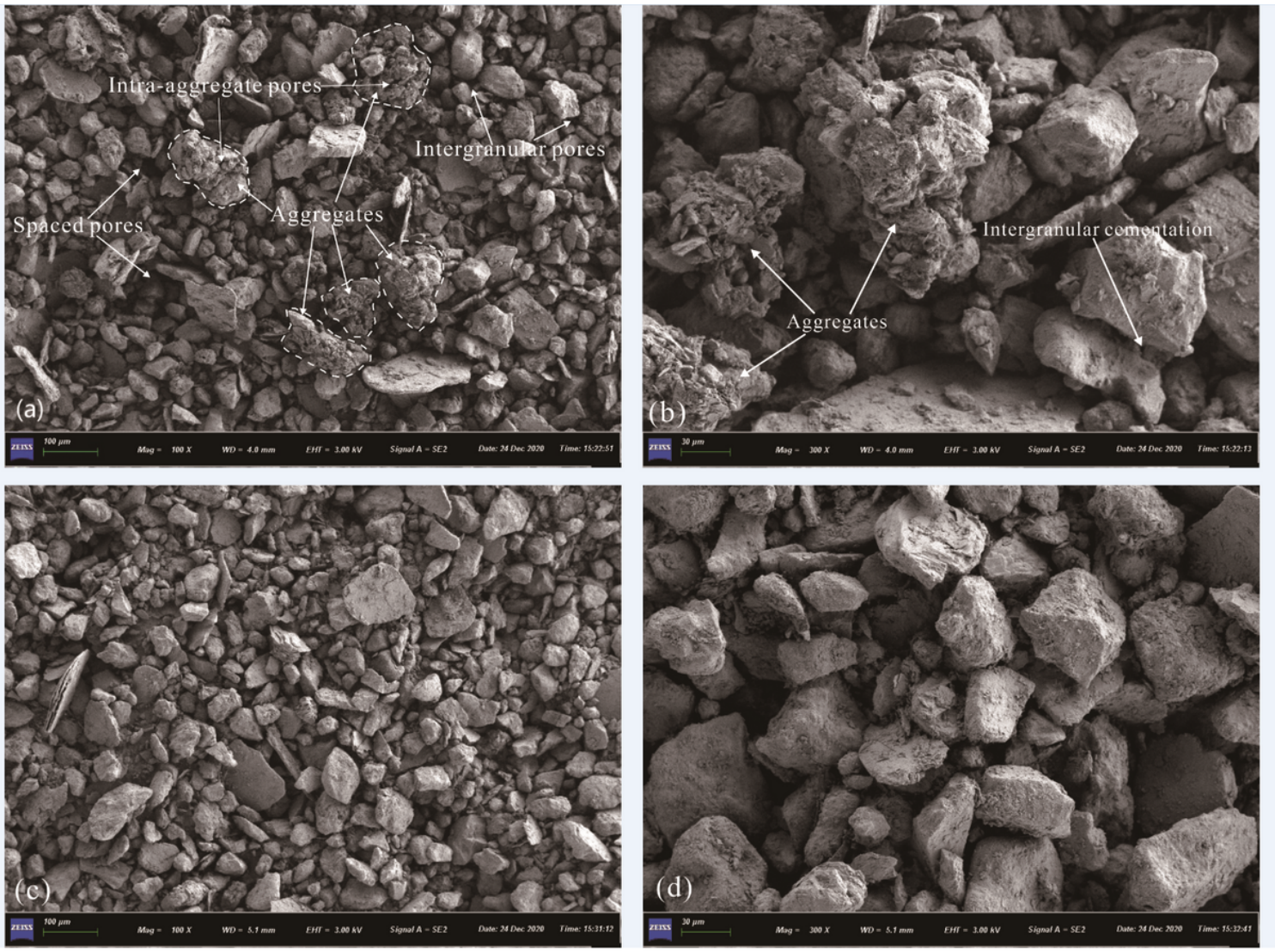

Figure 11

Photomicrographs of intact loess and saturated loess. Overall view:(a) intact loess, (c) saturated loess; detailed view: (b) intact loess, (d) saturated loess.

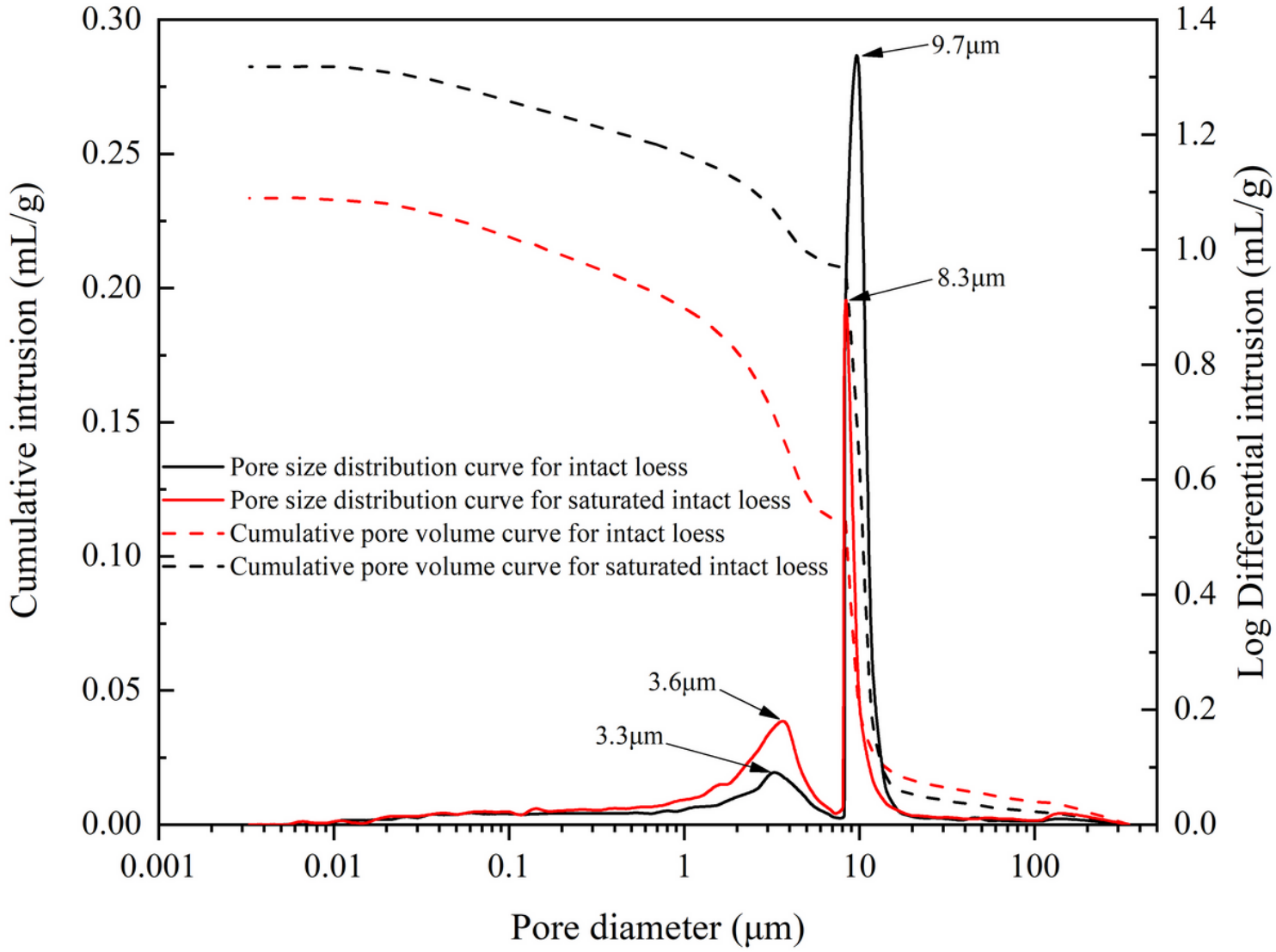

Figure 12

Pore size distribution curves and cumulative pore volume curves of intact loess and saturated loess.

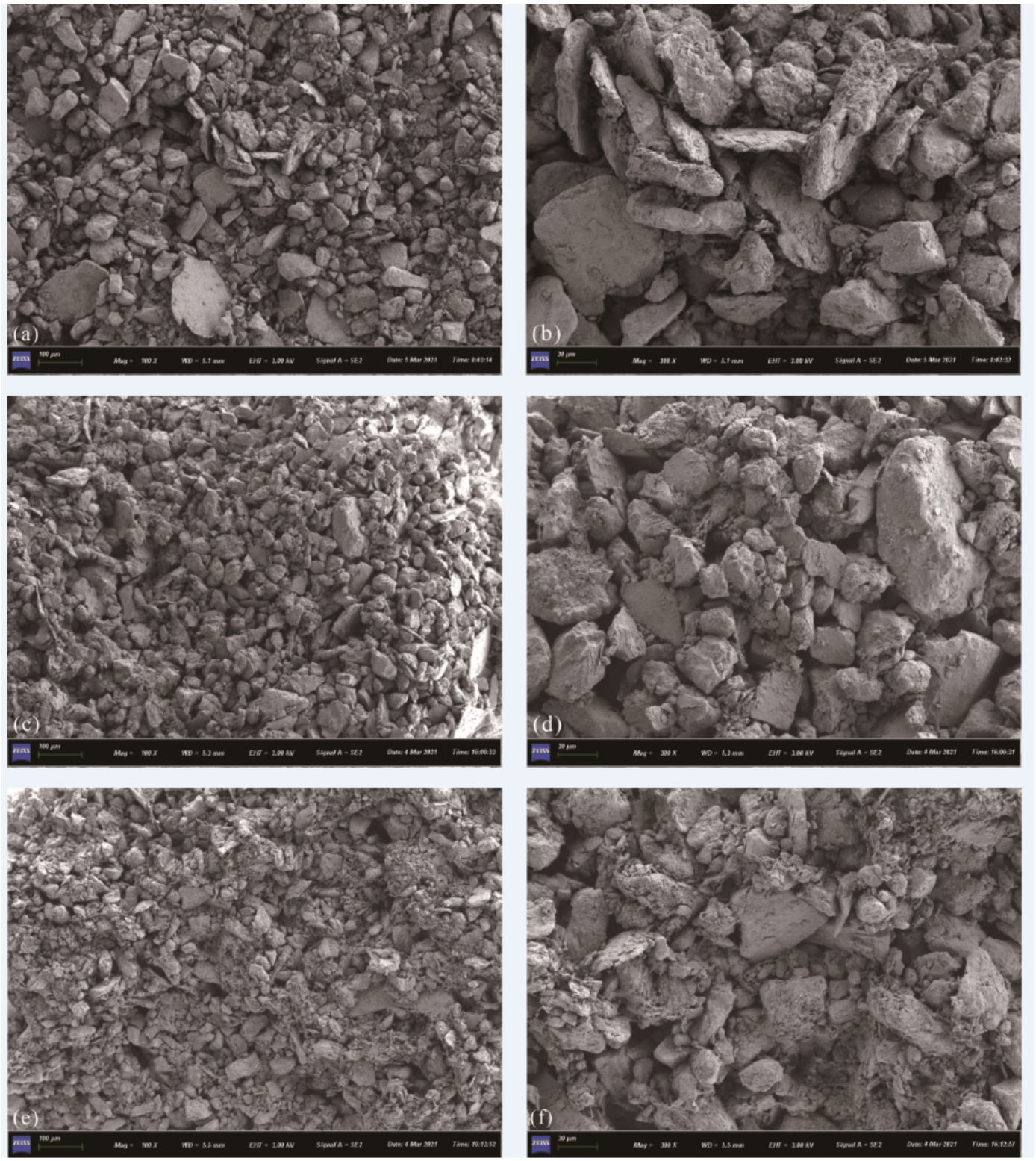

Figure 13

Photomicrographs of intact loess with different initial water content after compression: (a), (b) overall view and detailed view, w_0=7.14%; (c), (d) overall view and detailed view, w_0=18.03%; (e), (f) overall view and detailed view, w_0=35.02%.

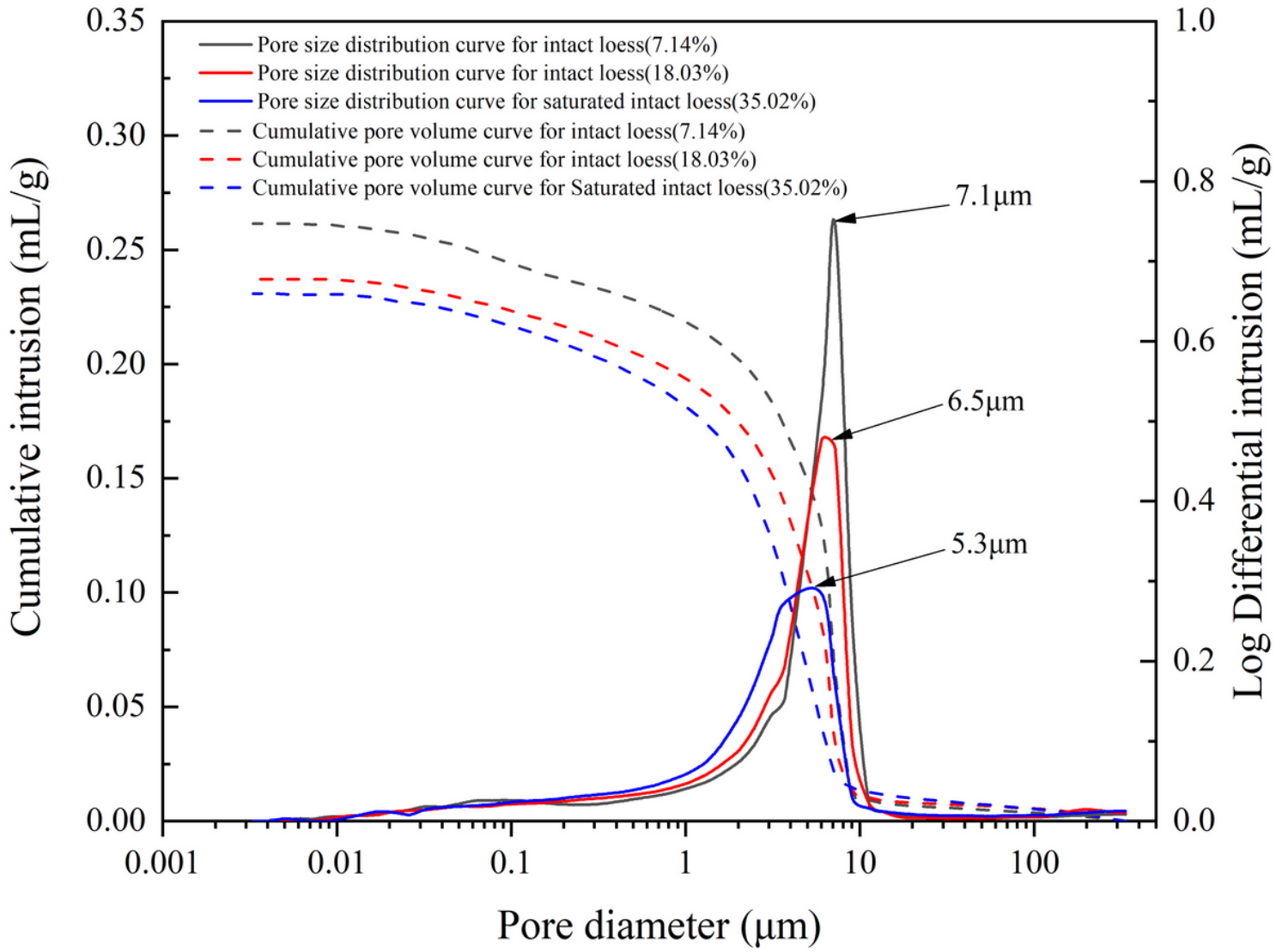

Figure 14

Pore size distribution curves and cumulative pore volume curves of intact loess with different initial water content after compression.